



ELSEVIER

Available online at www.sciencedirect.com

SCIENCE @ DIRECT®

Journal of Sound and Vibration 275 (2004) 489–513

JOURNAL OF
SOUND AND
VIBRATION

www.elsevier.com/locate/jsvi

Hydroelastic analysis of fluid storage tanks by using a boundary integral equation method

A. Ergin*, B. Uğurlu

Faculty of Naval Architecture and Ocean Engineering, Istanbul Technical University, Maslak, 80626, Istanbul, Turkey

Received 21 January 2003; accepted 1 July 2003

Abstract

This paper presents a boundary integral equation method in conjunction with the method of images, in order to investigate the dynamic behaviour (*wet* frequencies and associated mode shapes) of fluid containing structures. In the analysis of the linear fluid–structure system, it is assumed that the fluid is ideal, and fluid forces are associated with inertial effects of the contained fluid. This implies that the fluid pressure on the wetted surface of the structure is in phase with the structural acceleration. The *in vacuo* dynamic properties of the *dry* structure are obtained by using standard finite element software. In the *wet* part of the analysis, the fluid–structure interaction effects are calculated in terms of the generalized added mass coefficients by use of the boundary integral equation method together with the method of images in order to impose the $\Phi = 0$ boundary condition on the free surface. In this study, three different test cases are considered: (i) a clamped–free cylindrical tank with a rigid bottom; (ii) a flexible circular plate in a rigid cylindrical tank and (iii) a flexible cylindrical shell with flexible end plates (hermetic can). The fluid storage tanks in this investigation are assumed partially or completely filled with water. To assess the influence of the contained fluid on the dynamic characteristics, the *wet* natural frequencies and associated mode shapes are calculated. The predictions compare well with available experimental and numerical data.

© 2003 Elsevier Ltd. All rights reserved.

1. Introduction

Dynamic interaction between a structure and a fluid medium brings together all the aspects associated with both structural dynamics and fluid dynamics. When the structure is in contact with a fluid of comparable density, such as water, the fluid loading which depends on the structural surface motions will significantly alter the dynamic state of the structure from that of the *in vacuo* vibration. However, the fluid–structure interaction can be considered as *feedback*

*Corresponding author. Fax: +90-212-285-6454.

E-mail address: ergina@itu.edu.tr (A. Ergin).

coupling. In other words, the equations of structural and fluid motions must be solved simultaneously unless certain assumptions are made to uncouple them.

The dynamic fluid–structure interaction problems in which the fluid domain is modelled with finite elements are generally formulated using fluid particle displacement, pressure or velocity potential, etc. as the major unknown. These procedures are quite effective for problems involving a bounded fluid domain. For instance, Lim and Petyt [1] investigated the free vibration characteristics of a thin, circular cylindrical shell partially- or completely-filled with water, using displacement potential and displacement as the fundamental unknowns, respectively, in the fluid and structural domains. Alternatively, Olson and Bathe [2] used velocity potential as the major unknown in the fluid and presented a finite element method for solving fluid–structure interaction problems. Using appropriate variational formulations by means of the finite element method, Ohayon and Valid [3] and Morand and Ohayon [4] derived various symmetric matrix equations for the linear vibrations of elastic structures coupled to internal fluids. Mazúch et al. [5] used Ahmad shell elements with reduced integration for thin shells and quadratic fluid elements for an inviscid incompressible fluid, and calculated and measured the free vibration characteristics (i.e., natural frequencies, mode shapes, etc.) of a clamped–free cylindrical shell partially filled with water. More recently, Zhang et al. [6] presented a finite element method, based on Sanders’ non-linear thin shell theory and the classical potential flow theory, for the vibration of initially tensioned thin-walled orthotropic cylindrical tubes conveying fluid.

Boundary integral equation methods are also widely applied for the fluid flow, together with a finite element method for the structure displacements. For example, Röhr and Möller [7] described a hydroelastic vibration analysis method based on a combined finite element–boundary element procedure. Mysore et al. [8] used a finite element method to model an inflatable dam structure, and a boundary element technique to determine the behaviour of the fluid. Ergin et al. [9] studied the dynamic behaviour of a thin, horizontal cylindrical shell vibrating at fixed positions below a free surface in water of finite depth. By using a boundary element technique, they calculated the generalized fluid loading to assess the influence of free surface, rigid boundary and position of submerged cylinder on the dynamic characteristics of the shell structure. Nestegård and Mejlænder-Larsen [10] proposed a symmetric boundary integral equation method for the fluid flow, coupled with a finite element method for the structure displacements, and presented eigenfrequencies and associated mode shapes of partially submerged three-dimensional structures. More recently, Ergin and Temarel [11] proposed an approach based on a boundary integral equation method and the method of images, in order to calculate the fluid–structure interaction forces of a partially filled and/or submerged horizontal cylindrical shell. In their investigation they calculated the generalized fluid–structure interaction forces in terms of generalized added mass terms, and compared the calculated wet frequencies and mode shapes with experimental data found in the literature.

In this paper, the dynamic characteristics of fluid storage tanks are investigated using a boundary element method in conjunction with the method of images in order to impose an appropriate boundary condition on the fluid’s free surface. The structures considered in this study are (i) a clamped–free flexible cylindrical shell with a rigid bottom, (ii) a flexible bottom plate in a rigid cylindrical tank and (iii) a flexible cylindrical shell with flexible end plates (hermetic can). For all the test cases studied, the cylindrical structures are considered as partially or completely filled. The method employed in this study is already successfully applied to a partially liquid-filled and

submerged, horizontal cylindrical shell (see Ergin and Temarel [11]). In the study of Ergin and Temarel [11], appropriate boundary conditions on the fluid–structure interface (i.e., the normal component of fluid velocity must coincide with that of the structure) and on the free surface (i.e., $\Phi = 0$) were imposed. But, no fluid–structure interface condition was employed on the circular ends of the shell structure. Thus, this study provides an extension to Ergin and Temarel [11] by accounting for the effects of rigid boundaries, such as rigid tank bottom or rigid tank wall, and flexible end plates in the evaluation of the fluid loading. In this investigation, it is assumed that the fluid is ideal, i.e., inviscid, incompressible and its motion is irrotational. Furthermore, the fluid forces are associated with the inertial effect of the fluid, i.e., the fluid pressure on the wetted surface of the structure is in phase with the structural acceleration. In the analysis, it is assumed that the flexible structure vibrates in its in vacuo eigenmodes when it is in contact with fluid, and that each mode gives rise to a corresponding surface pressure distribution on the wet part of the structure. The in vacuo dynamic analysis entails the vibration of the elastic structure in the absence of any external force and structural damping, and the corresponding dynamic characteristics (e.g., natural frequencies and principal mode shapes) of the structure were obtained by using a standard finite element software (i.e., ANSYS [12]). At the fluid–structure interface, continuity considerations require that the normal velocity of the fluid is equal to that of the structure. The normal velocities on the wetted shell and plate surfaces are expressed in terms of modal structural displacements, obtained from the in vacuo dynamic analysis. By using the boundary integral equation method the fluid pressure is eliminated from the problem, and using the method of images (i.e., imposing an appropriate free surface boundary condition, namely $\Phi = 0$), the fluid–structure interaction forces are calculated solely in terms of generalized added mass coefficients. During this analysis, the wet surfaces (flexible and rigid) are idealized by using appropriate boundary elements, referred to as hydrodynamic panels. The generalized structural mass matrix is merged with the generalized added mass matrix and then the total generalized mass matrix is used in solving the eigenvalue problem. To assess the influence of the contained fluid on the dynamic response behaviour of the elastic structure, the wet natural frequencies and associated mode shapes are calculated. A comparison of the predicted dynamic characteristics (i.e., wet natural frequencies and associated mode shapes) with available experimental measurements and numerical data shows very good agreement.

2. Mathematical model

2.1. Equation of motion

A general three-dimensional structure may be represented as an assemblage of discrete finite elements being interconnected at nodal points on the element boundaries. For small deformations, the displacement measured in a local co-ordinate system may be approximated by an expansion over a finite number of displacements selected at the nodes in the discretized structure as

$$\mathbf{u}_e(\xi, \eta, \zeta) = \mathbf{N}_e(\xi, \eta, \zeta)\mathbf{U}, \quad (1)$$

where the subscript e denotes the e th element. \mathbf{N}_e is a matrix describing the displacements within the element in terms of independent variables (i.e., co-ordinates, ξ, η, ζ). It should be noticed that

\mathbf{N}_e is expanded to accommodate all global displacements. The matrix \mathbf{U} accommodates global displacements at all the nodal points.

The equation of dynamic equilibrium of the structure can be obtained by applying the principle of virtual displacements in conjunction with D'Alembert's principle [13] as

$$\mathbf{M}\ddot{\mathbf{U}} + \mathbf{C}_V\dot{\mathbf{U}} + \mathbf{K}\mathbf{U} = \mathbf{P}, \quad (2)$$

where \mathbf{M} , \mathbf{C}_V and \mathbf{K} denote the $(N \times N)$ mass, structural damping and stiffness matrices, respectively, and they may be expressed as follows

$$\begin{aligned} \mathbf{M} &= \sum_{e=1}^N \int \int \int_{\Omega_e} \rho_e \mathbf{N}_e^T \mathbf{N}_e \, d\Omega_e, & \mathbf{C}_V &= \sum_{e=1}^N \int \int \int_{\Omega_e} \kappa_e \mathbf{N}_e^T \mathbf{N}_e \, d\Omega_e, \\ \mathbf{K} &= \sum_{e=1}^N \int \int \int_{\Omega_e} \mathbf{B}_e^T \chi_e \mathbf{B}_e \, d\Omega_e, \end{aligned} \quad (3-5)$$

where the matrix \mathbf{B}_e contains prescribed functions of the co-ordinates and χ_e is a matrix of elastic constants. ρ_e and κ_e are, respectively, the density and damping property parameters of the e th element. The $(N \times 1)$ matrices \mathbf{U} , $\dot{\mathbf{U}}$ and $\ddot{\mathbf{U}}$ represent the structural displacements, velocities and accelerations respectively, and the $(N \times 1)$ column matrix \mathbf{P} denotes the external forces acting on the structure. N is the number of degrees of freedom assigned to the structure.

2.2. In vacuo analysis

In the in vacuo analysis, the structure is assumed to vibrate in the absence of any structural damping and external forces reducing Eq. (2) to the form

$$\mathbf{M}\ddot{\mathbf{U}} + \mathbf{K}\mathbf{U} = \mathbf{0}. \quad (6)$$

The form of Eq. (6) suggests that one can express the trial solution as

$$\mathbf{U} = \mathbf{D}e^{i\omega t}. \quad (7)$$

Using Eq. (7) in Eq. (6) and cancelling the common factor $e^{i\omega t}$, one obtains the equation

$$(-\omega^2 \mathbf{M} + \mathbf{K})\mathbf{D} = \mathbf{0}. \quad (8)$$

This equation describes the simple harmonic oscillations of the free undamped structure, and the in vacuo principal modes and natural frequencies are determined from the associated *eigenvalue* problem.

2.3. Generalized equation of motion

The displacement field of the structure may be expressed as the sum of the displacements in the principal modes [14],

$$\mathbf{U} = \mathbf{D}\mathbf{p}(t), \quad (9)$$

where \mathbf{D} is the modal matrix whose columns are the in vacuo, undamped mode vectors of the structure. \mathbf{p} is the principal co-ordinates matrix. By substituting Eq. (9) into Eq. (2) and pre-multiplying by \mathbf{D}^T , the following generalized equation in terms of the principal co-ordinates of the

structure is obtained:

$$\mathbf{a}\ddot{\mathbf{p}}(t) + \mathbf{b}\dot{\mathbf{p}}(t) + \mathbf{c}\mathbf{p}(t) = \mathbf{Q}(t), \tag{10}$$

where \mathbf{a} , \mathbf{b} , \mathbf{c} denote the generalized mass, damping and stiffness matrices, respectively, and are defined as

$$\mathbf{a} = \mathbf{D}^T \mathbf{M} \mathbf{D}, \quad \mathbf{b} = \mathbf{D}^T \mathbf{C}_V \mathbf{D}, \quad \mathbf{c} = \mathbf{D}^T \mathbf{K} \mathbf{D}, \quad \mathbf{Q} = \mathbf{D}^T \mathbf{P}. \tag{11}$$

The generalized force matrix, $\mathbf{Q}(t)$ represents the fluid–structure interaction, $\mathbf{Z}(t)$, and all other external forces, $\mathbf{\Xi}(t)$.

2.4. Formulation of the fluid problem

The fluid is assumed ideal, i.e., inviscid and incompressible, and its motion is irrotational and there exists a fluid velocity vector, \mathbf{v} , which can be defined as the gradient of the velocity potential function Φ as

$$\mathbf{v}(x, y, z, t) = \nabla \Phi(x, y, z, t), \tag{12}$$

where Φ satisfies Laplace’s equation

$$\nabla^2 \Phi(x, y, z, t) = 0, \tag{13}$$

throughout the fluid domain.

For the structure vibrating with frequency ω , the response of the structure may be expressed in terms of principal co-ordinates as $\mathbf{p}(t) = \mathbf{p}_0 e^{i\omega t}$, and thus the velocity potential function Φ_r due to the deformed shape of the structure in the r th modal vibration may be written as (see, for instance, Ergin and Temarel [11] and Amabili et al. [15])

$$\Phi_r(x, y, z, t) = i\omega \phi_r(x, y, z) p_r e^{i\omega t}, \quad r = 1, 2, \dots, M, \tag{14}$$

where M represents the number of modes of interest, and p_r is the amplitude of the r th principal co-ordinate.

On the wetted surface of the vibrating structure the fluid normal velocity must be equal to the normal velocity on the structure and this condition for the r th modal vibration can be expressed as

$$-\partial \phi_r / \partial \mathbf{n} = \mathbf{u}_r \cdot \mathbf{n}, \tag{15}$$

where \mathbf{u}_r is the r th modal displacement vector of the median surface of the elastic structure and \mathbf{n} is the unit normal vector on the wetted surface and points into the region of interest. However, at the fluid–rigid body interface, the condition (15) takes the form

$$-\partial \phi_r / \partial \mathbf{n} = 0. \tag{16}$$

In this study, it is assumed that the elastic structure vibrates at relatively high frequencies so that the effect of surface waves can be neglected. Therefore, the free surface condition (infinite frequency limit condition) for ϕ_r can be approximated by

$$\phi_r = 0, \quad \text{on the free surface.} \tag{17}$$

The method of images [11,16] may be used, as shown in Fig. 1, to satisfy this condition. By adding an imaginary boundary region, the condition given by Eq. (17) at the horizontal surface can be omitted; thus the problem is reduced to a classical Neumann case. It should also be noted that the

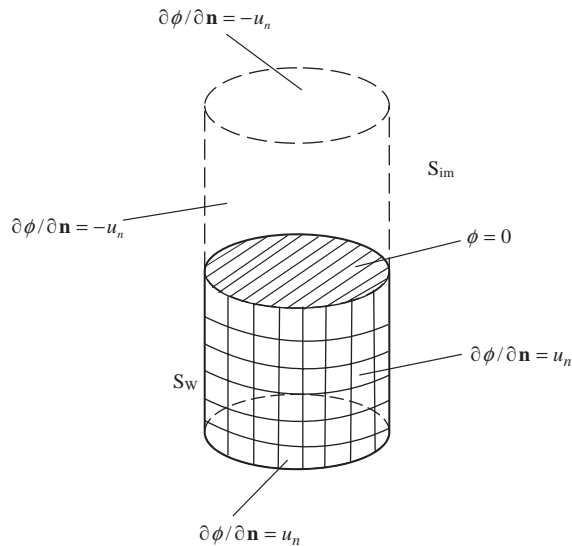


Fig. 1. Wetted surface and image boundary for a partially-filled structure.

normal fluid velocity cannot be arbitrarily specified. It has to satisfy the incompressibility condition

$$\int \int_{S_w + S_{im}} \frac{\partial \phi_r}{\partial \mathbf{n}} dS = 0, \tag{18}$$

where S_w and S_{im} represent the wetted and image surfaces respectively (see Fig. 1).

Using the Bernoulli’s equation and neglecting the second order terms, the dynamic fluid pressure on the elastic structure due to the r th modal vibration becomes

$$P_r(x, y, z, t) = -\rho \partial \Phi_r / \partial t. \tag{19}$$

Substituting Eq. (14) into (19), the following expression for the pressure is obtained,

$$P_r(x, y, z, t) = \rho \omega^2 \phi_r(x, y, z) p_r e^{i\omega t}. \tag{20}$$

The k th component of the generalized fluid–structure interaction force due to the r th modal vibration of the elastic structure can be expressed in terms of the pressure acting on the wetted surface of the structure as

$$Z_{kr}(t) = \int \int_{S_w} P_r(x, y, z, t) \mathbf{u}_k \mathbf{n} dS = p_r e^{i\omega t} \int \int_{S_w} \rho \omega^2 \phi_r \mathbf{u}_k \mathbf{n} dS. \tag{21}$$

The generalized added mass term A_{kr} can be defined as

$$A_{kr} = \rho \int \int_{S_w} \phi_r \mathbf{u}_k \mathbf{n} dS. \tag{22}$$

Therefore, the generalized fluid–structure interaction force component, Z_{kr} , can be rewritten as

$$Z_{kr}(t) = A_{kr} \omega^2 p_r e^{i\omega t} = -A_{kr} \ddot{p}_r(t). \tag{23}$$

2.5. Numerical evaluation of deformation potential ϕ

The deformation potential, ϕ , in a three-dimensional inviscid flow field due to the oscillating elastic structure can be expressed by means of a distribution of unknown source strength, σ , over the wetted and image surfaces of the structure (see, for example, [17,18]) in the form

$$\phi(\mathbf{r}) = \int \int_{S_w+S_{im}} \frac{\sigma(\mathbf{r}_0)}{R(\mathbf{r}, \mathbf{r}_0)} dS, \tag{24}$$

where

$$R = [(x - x_0)^2 + (y - y_0)^2 + (z - z_0)^2]^{1/2},$$

and $\mathbf{r} = (x, y, z)$ denotes the position vector of the field point within the fluid, $\mathbf{r}_0 = (x_0, y_0, z_0)$ is the position vector of a source point on the wetted/image surface of the structure.

Substituting boundary conditions (15) and (16) into (24), the unknown strength σ can be determined from the set of algebraic equations

$$2\pi\sigma_i - \sum_{j=1}^N \sigma_j \int \int_{\Delta S_j} \frac{\partial}{\partial \mathbf{n}} \left[\frac{1}{R(\mathbf{r}_i, \mathbf{r}_j)} \right] dS = u_{ni}, \quad i = 1, 2, \dots, N, \tag{25}$$

where ΔS_j represents the area of the j th panel, N is the number of panels required to discretize the wetted and image surfaces and u_{ni} denotes the modal displacement in the direction of the normal at the control point (x_i, y_i, z_i) of the i th panel.

2.6. Calculation of wet frequencies and mode shapes

The generalized equation of motion for the dynamic fluid–structure interaction system assuming free vibrations with no structural damping is

$$[-\omega^2(\mathbf{a} + \mathbf{A}) + \mathbf{c}]\mathbf{p} = \mathbf{0}, \tag{26}$$

where \mathbf{a} and \mathbf{c} denote the generalized structural mass and stiffness matrices respectively. The matrix \mathbf{A} represents the generalized added mass coefficients.

Solving the *eigenvalue* problem, expressed by Eq. (26), the *wet* frequencies and associated mode shapes of the elastic structure in contact with fluid are obtained. To each *wet* frequencies ω_r , there is a corresponding *wet* eigenvector $\mathbf{p}_{or} = \{p_{r1}, p_{r2}, \dots, p_{rm}\}$ satisfying Eq. (26). The corresponding uncoupled mode shapes for the structure partially or totally in contact with fluid are obtained as

$$\bar{\mathbf{u}}_r(x, y, z) = \{\bar{u}_r, \bar{v}_r, \bar{w}_r\} = \sum_{j=1}^M \mathbf{u}_j(x, y, z)\mathbf{p}_{rj}, \tag{27}$$

where $\mathbf{u}_j(x, y, z) = \{u_j, v_j, w_j\}$ denote the in vacuo mode shapes of the elastic structure and M the number of mode shapes included in the analysis.

3. Numerical results and comparisons

A right-handed Cartesian co-ordinate system, xyz , is adopted in the present study and it is shown in Fig. 2 for the cylindrical tank partially filled with fluid. The co-ordinate system is fixed at the base with its origin at O . The x -axis lies along the length L , and coincides with the centreline of the cylindrical tank. The filling depth and radius are denoted by d and r , respectively.

The *wet* frequencies and associated uncoupled *wet* modes were calculated by using Eqs. (26) and (27), respectively. It should be noted that the fluid–structure interaction forces associated with the inertial effect of the fluid do not have the same spatial distribution as those of the in vacuo modal forms. Consequently, this produces hydrodynamic coupling between the modes. This coupling effect is introduced into Eq. (26) through the added mass matrix \mathbf{A} .

3.1. A clamped–free cylindrical shell with a rigid bottom

A vertical clamped–free cylindrical shell with a rigid bottom is chosen to demonstrate the applicability of the aforementioned theory to structures partially filled such as liquid storage

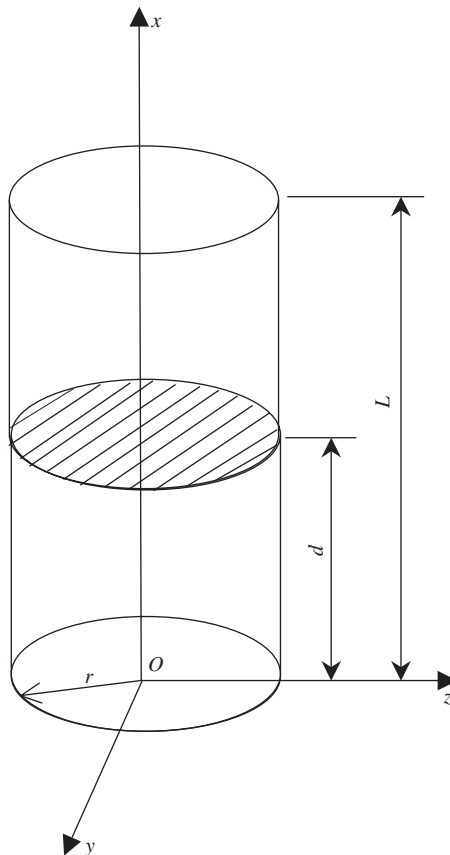


Fig. 2. Partially-filled cylindrical tank.

tanks. The cylindrical shell is of length $L = 231$ mm, radius $r = 77.25$ mm, and thickness $t = 1.5$ mm, and experimentally and numerically studied by Mazúch et al. [5]. The shell structure is made of steel, and has the material characteristics: Young's modulus $E = 205$ GPa, Poisson ratio $\nu = 0.3$, mass density $\rho_s = 7800$ kg/m³. Fresh water is used as the contained fluid with a density of $\rho_f = 1000$ kg/m³.

The in vacuo dynamic characteristics of the clamped–free cylindrical shell were obtained by use of ANSYS [12], a standard finite-element software. This produces information on the natural frequencies and principal mode shapes of the *dry* structure. In these calculations, the cylindrical shell was discretized with four-noded quadrilateral shell elements, including both membrane and bending stiffness influences.

In a preliminary calculation, 512 elements were distributed over the shell structure. The distribution over the clamped–free cylindrical shell consists of 32 equally spaced elements around the circumference and 16 equally spaced elements along the shell structure. To test the convergence of the calculated dynamic properties, i.e., natural frequencies and principal mode shapes, the number of elements over the cylindrical shell surface was increased first to 1152—48 elements around the circumference and 24 elements along the shell. In a final test of idealization, the number of elements was increased to 64 and 32, respectively, around the circumference and along the cylindrical shell. Therefore, a total number of 2048 elements were distributed over the shell structure in this final idealization. Table 1 shows the experimental measurements of Mazúch et al. [5], and the predicted natural frequencies obtained from ANSYS in this study. The differences in the results indicate that the calculated values are converging with increasing number of elements. The results of the final idealization (2048 elements) compare very well with the experimental measurements of Mazúch et al. [5], except for the mode shape ($m = 1$ and $n = 2$), and they were adopted for the in vacuo dynamic characteristics of the vertical clamped–free cylindrical shell. The mode shapes of the cylindrical shell are identified with the number of standing waves around the circumference, n , and the axial mode number, m .

To test the convergence of the hydrodynamic predictions, various numbers of hydrodynamic panels were distributed around the circumference and along the length of the wetted surface of the cylindrical shell. In addition a limited number of hydrodynamic panels was also distributed over

Table 1
Convergence of FEM natural frequencies (in vacuo) for clamped–free cylindrical shell (Hz)

Mode (m, n)	512 elements idealization	1152 elements idealization	2048 elements idealization	Experiment [5]
1,3	635.8	634.6	634.2	616
1,2	813.5	814.0	814.2	708
1,4	953.8	950.5	949.2	945
1,5	1490.4	1484.9	1482.5	1479
2,4	1657.4	1651.5	1649.8	1628
1,1	1823.2	1825.0	1825.6	—
2,5	1948.2	1842.5	1840.3	1851
2,3	2036.6	2031.4	2029.9	1969
1,6	2168.7	2160.7	2156.8	2151
2,6	2396.9	2388.9	2385.8	—

the wetted rigid bottom surface, in order to impose the boundary condition $\partial\phi/\partial\mathbf{n} = 0$ on the wetted rigid surface. For the completely-filled shell, three different idealizations of panel distribution were considered (see Table 2). In the first idealization, the distribution involved 32 equally spaced quadratic panels around the circumference and 16 equally spaced quadratic panels along the wetted cylindrical shell, and 193 quadratic panels over the wetted rigid bottom. Thus, a total number of 705 panels was adopted in this idealization. In a second idealization, 1441 hydrodynamic panels were used—the number of panels around the wetted circumference and along the shell structure was, respectively, increased to 48 and 24. 289 hydrodynamic panels, on the other hand, were distributed over the wetted rigid bottom surface. Finally, for a third idealization, the total number of panels distributed over the wetted surfaces was increased to 2433—64 panels around the circumference, 32 panels along the wetted cylinder, and 385 panels over the wetted rigid bottom. Table 2 shows the convergence of the predicted wet natural frequency values with increasing number of hydrodynamic panels for the completely-filled clamped–free cylindrical shell. The differences between the predictions based on the last idealization and experimental measurements of Mazúch et al. [5] are reasonably small (see Table 2). Therefore, it may be said that the final idealization (2433 panels idealization) adequately represents the displaced shapes of the completely-filled structure. The convergence tests were also performed for different filling ratios. For instance, for the filling ratios $d/L = 0.2, 0.5$ and 0.7 , the converged results were obtained, respectively, by use of 769, 1345 and 1729 hydrodynamic panels distributed over the wetted shell and rigid bottom surfaces. In addition convergence studies were also carried out to establish the number of in vacuo modes needed for the predictions presented. A maximum number of $M = 40$ in vacuo modes was included in the analysis.

The uncoupled modes and associated frequencies of the partially filled clamped–free cylindrical shell are obtained by solving the eigenvalue problem, Eq. (26). The results of the present study are compared with the experimental measurements and finite element calculations of Mazúch et al. [5] in Table 3, for the first ten modes. The predicted frequencies show similar trends with the experimental and numerical data of Mazúch et al. [5]. That is to say that the resonance frequencies increase with decreasing filling ratio (d/L). Therefore, the highest frequencies are obtained for the empty shell (see Table 3). However, there are differences between the results of this study and

Table 2
Convergence of wet natural frequencies for completely-filled clamped–free cylindrical shell (Hz)

Mode (m, n)	705 panels idealization	1441 panels idealization	2433 panels idealization	Experiment [5]
1,3	410.3	403.1	400.7	388
1,2	486.6	482.9	481.1	421
1,4	660.5	642.1	635.3	628
1,5	1097.4	1055.0	1039.7	1027
1,1	1048.5	1044.3	1041.9	—
2,4	1159.2	1124.1	1111.8	1094
2,3	1325.7	1297.9	1288.0	1245
2,5	1378.1	1324.3	1305.0	1299
1,6	1685.9	1604.8	1574.3	1546
2,6	1884.4	1795.3	1762.4	1748

Table 3
Comparisons of *dry* and *wet* natural frequencies for clamped–free cylindrical shell (Hz)

Mode (<i>m, n</i>)	Dry analysis			Wet analysis								
	This study	FEA [5]	Experiment [5]	<i>d/L</i> = 0.5			<i>d/L</i> = 0.7			<i>d/L</i> = 1		
				This study	FEA [5]	Experiment [5]	This study	FEA [5]	Experiment [5]	This study	FEA [5]	Experiment [5]
1,3	634.2	633	616	608.9	609.4	542.0	543.1	522	400.7	400.6	388	
1,2	814.2	814	708	769.3	771.1	669.8	672.7	582	481.1	482.1	421	
1,4	949.2	947	945	908.4	908.8	806.8	806.0	798	635.3	633.2	628	
1,5	1482.5	1480	1479	1351.8	1352.8	1195.5	1188.4	1196	1039.7	1033.0	1027	
2,4	1649.8	1648	1628	1308.4	1303.9	1261.4	1253.2	1244	1111.8	1110.6	1094	
1,1	1825.6	1827	—	1654.7	1654.4	1407.3	1407.4	—	1041.9	1038.6	—	
2,5	1840.3	1839	1851	1571.3	1565.8	1557.7	1553.8	1546	1305.0	1304.2	1299	
2,3	2029.9	2029	1969	1519.9	1515.2	1434.0	1425.3	1394	1288.0	1286.9	1245	
1,6	2156.8	2154	2151	1843.5	1842.7	1693.6	1679.7	—	1574.3	1561.3	1546	
2,6	2385.8	—	—	2189.6	2189.0	2119.7	—	—	1762.4	1762.6	1748	

those of Mazúch et al. [5]. These differences lie in the range between no difference and 3.8% in comparison with the experimental data, except for the mode shape ($m = 1, n = 2$), and between no difference and 0.8% when compared with the finite element results of Mazúch et al. [5]. For the mode shape ($m = 1, n = 2$), there is approximately 15% difference between the present results and experimental measurements for all the filling ratios, including the empty shell ($d/L = 0$). Mazúch et al. [5] also observed a similar discrepancy between their predictions and experimental measurements for the above mentioned mode shape ($m = 1, n = 2$) (see Table 3). These discrepancies may be due to the sensitivity of the lower order modes to the boundary conditions existing in the experiment. It was also reported by Mazúch et al. [5] that the end of the cylindrical shell at the base was, probably, not so perfectly fixed in the experiment as was supposed in the finite element model.

Fig. 3 shows the predicted wet natural frequencies of the clamped–free cylindrical shell as a function of filling ratio (d/L) for various circumferential wave numbers and axial mode numbers. As can be observed from Fig. 3, the frequencies decrease with increasing filling ratio (d/L). The lowest *wet* frequencies, therefore, occurred for the filling ratio $d/L = 1$. On the other hand, it can be realized by comparing Figs. 3(a–e) that the *wet* natural frequencies increase with increasing number of axial modes, m , for a given number of circumferential waves, n . Thus, as seen in Fig. 3(e), the highest frequencies were calculated for the axial mode number $m = 5$.

Figs. 4 and 5 show, respectively, the predicted mode shapes ($m = 1, n = 3$) and ($m = 1, n = 5$) for the filling ratios $d/L = 0, 0.2, 0.4, 0.6, 0.8$ and 1. As seen in Fig. 4, the mode shape ($m = 1, n = 3$) is only slightly influenced by water, and the mode shape resembles itself when the water level increases. On the other hand, the mode shape with $m = 1$ and $n = 5$ in Fig. 5 shows similar displacement characteristics for all the filling ratios. However, they are more influenced by the presence of water.

The generalized added mass values associated with the distortional in vacuo modes are a function of the waves around the circumference and the number of waves along the cylinder. They

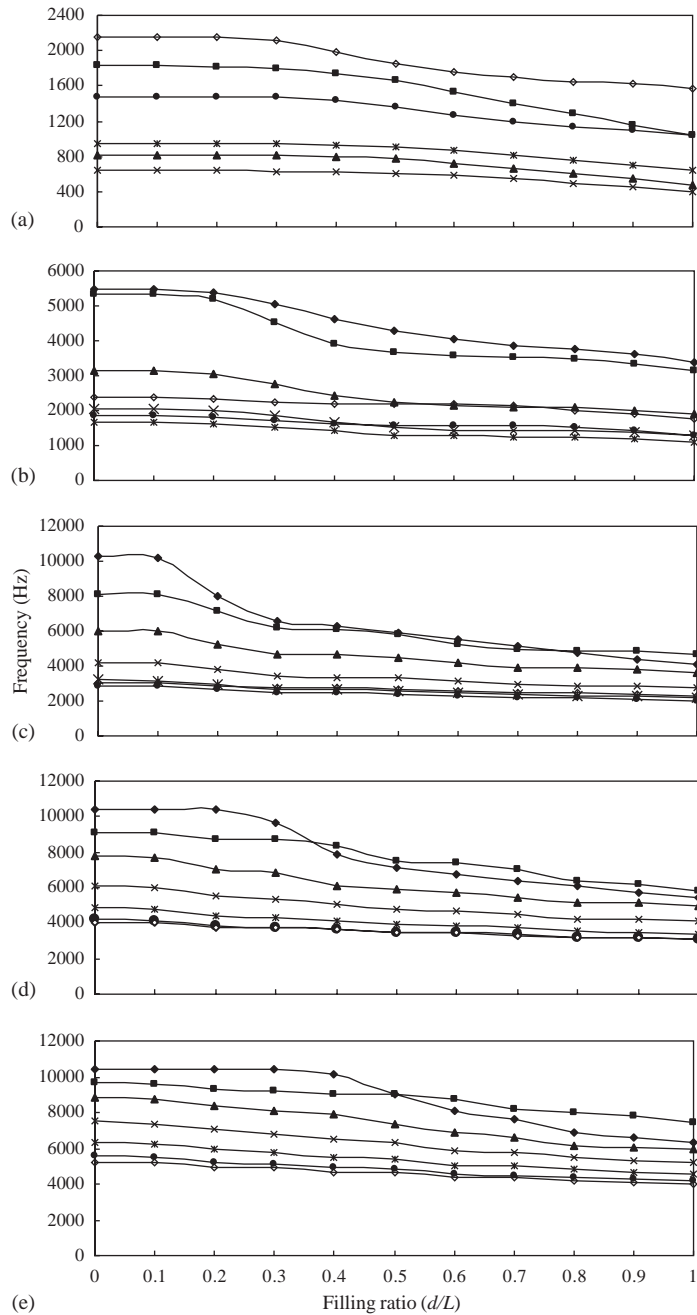


Fig. 3. Wet frequencies of clamped-free cylindrical shell as a function of filling ratio (d/L): (a) $m = 1$; (b) $m = 2$; (c) $m = 3$; (d) $m = 4$; (e) $m = 5$. Key: $-\blacklozenge-$, $n = 0$; $-\blacksquare-$, $n = 1$; $-\blacktriangle-$, $n = 2$; $-\times-$, $n = 3$; $-\ast-$, $n = 4$; $-\bullet-$, $n = 5$; $-\diamond-$, $n = 6$.

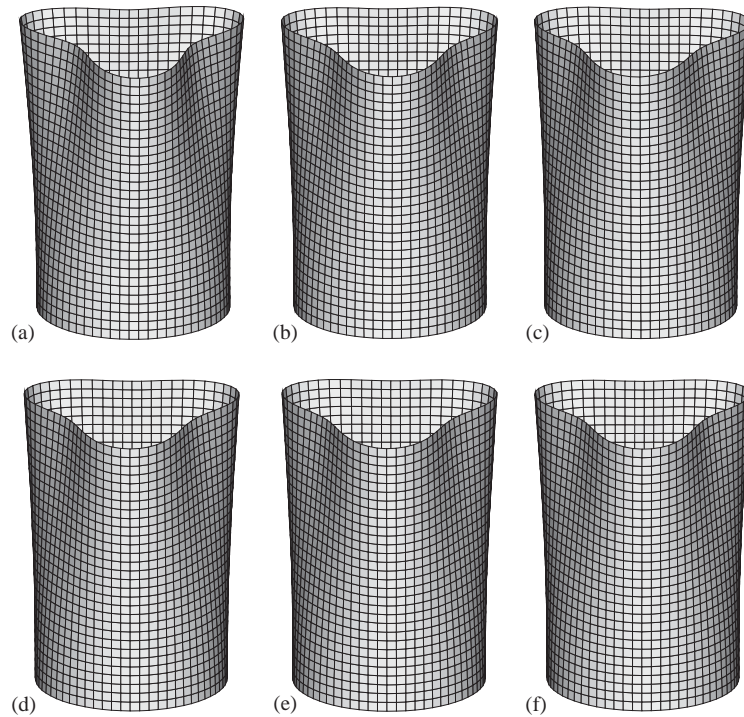


Fig. 4. Predicted mode shapes with $m = 1$ and $n = 3$: (a) empty shell, $d/L = 0$; (b) $d/L = 0.2$; (c) $d/L = 0.4$; (d) $d/L = 0.6$; (e) $d/L = 0.8$; (f) $d/L = 1$.

gradually decrease with increasing number of circumferential waves, n . The calculated generalized added mass values, for the half-filled clamped–free shell, are presented in Table 4 for the first 12 in vacuo modes shapes. Table 4 also shows the hydrodynamic coupling between the in vacuo mode shapes. The generalized added mass values in Table 4 were obtained for the in vacuo modes scaled to a generalized structural mass of 1 kg m^2 . In the method presented, it is assumed that the structure preserves its in vacuo principal mode shapes in the fluid and that each mode gives rise to the pressure distribution of the flexible structure. However, the hydrodynamic forces associated with the inertial effect of the contained fluid do not necessarily have the same spatial distribution as those of the in vacuo principal modes. Consequently, this produces hydrodynamic coupling between the in vacuo modes. From Table 4, it is seen that the generalized added mass matrix is symmetric and the cross-coupling terms are generally negligible in comparison with the diagonal ones. However, as seen from Table 4, there is considerable coupling between some of the in vacuo principal modes (for example, between modes 1–3 and 2–3, or 1–2 and 2–2).

3.2. A flexible bottom plate in a rigid circular cylindrical tank partially filled with water

In a second test study, a circular plate is considered as a flexible bottom of a rigid cylindrical tank filled with water. The flexible bottom plate used in the calculations is made of steel and has the geometric and material properties: radius $r = 0.144 \text{ m}$, thickness $t = 0.002 \text{ m}$, Young's modulus $E = 206 \text{ GPa}$, the Poisson ratio $\nu = 0.25$, mass density $\rho_s = 7850 \text{ kg/m}^3$. The rigid

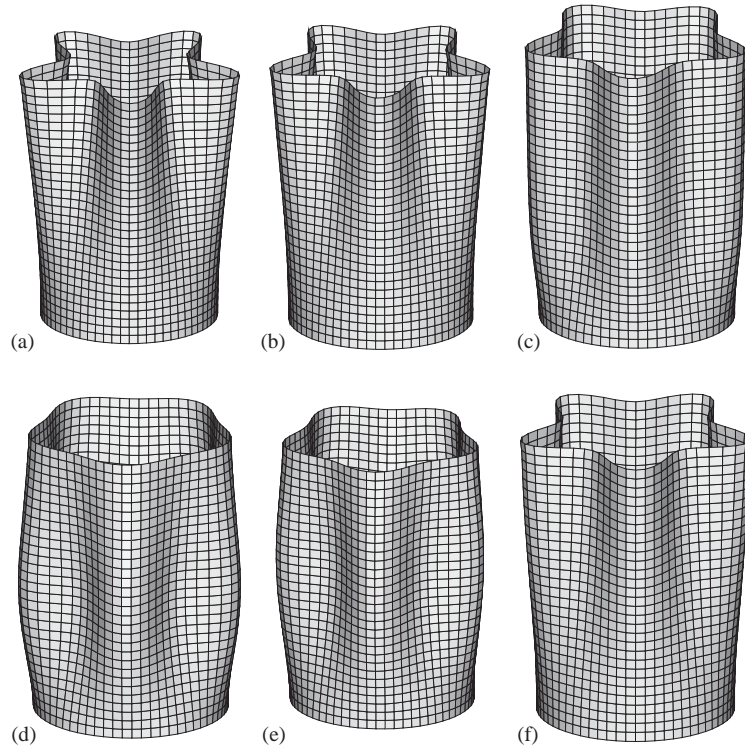


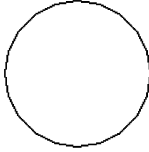
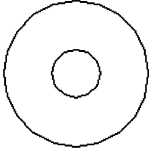
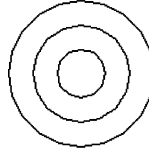
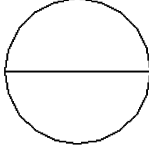
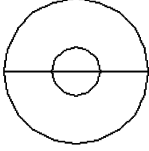
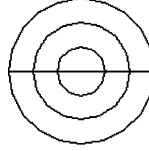
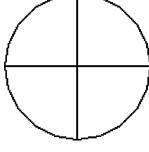
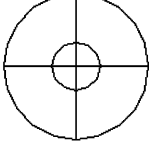
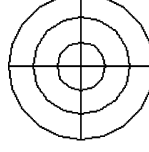
Fig. 5. Predicted mode shapes with $m = 1$ and $n = 5$: (a) empty shell, $d/L = 0$; (b) $d/L = 0.2$; (c) $d/L = 0.4$; (d) $d/L = 0.6$; (e) $d/L = 0.8$; (f) $d/L = 1$.

Table 4
Generalized added mass coefficients (kg m^2) of half-filled clamped–free cylindrical shell

Mode (m, n)	1,3	1,2	1,4	1,5	2,4	1,1	2,5	2,3	1,6	2,6	2,2	2,1
1,3	0.7772	0.0000	0.0000	0.0000	0.0000	0.0000	-0.0001	2.3756	0.0000	0.0000	0.0000	0.0000
1,2	0.0000	1.1158	0.0000	0.0000	0.0000	0.0000	0.0000	0.0000	0.0000	0.0000	3.2503	0.0000
1,4	0.0000	0.0000	0.6552	0.0000	-1.9227	0.0000	0.0000	0.0000	0.0000	0.0000	0.0000	0.0000
1,5	0.0000	0.0000	0.0000	0.6481	0.0000	-0.0001	1.3055	0.0001	0.0000	0.0000	0.0000	-0.0001
2,4	0.0000	0.0000	-1.9227	0.0000	6.0239	0.0000	0.0000	0.0000	0.0000	0.0000	0.0000	0.0000
1,1	0.0000	0.0000	0.0000	-0.0001	0.0000	1.8304	-0.0002	0.0000	0.0000	0.0000	0.0000	3.8686
2,5	-0.0001	0.0000	0.0000	1.3055	0.0000	-0.0002	4.9435	-0.0001	0.0000	0.0000	0.0000	0.0002
2,3	2.3756	0.0000	0.0000	0.0001	0.0000	0.0000	-0.0001	7.7360	0.0000	0.0000	0.0000	0.0000
1,6	0.0000	0.0000	0.0000	0.0000	0.0000	0.0000	0.0000	0.0000	0.6814	0.0053	0.0000	0.0000
2,6	0.0000	0.0000	0.0000	0.0000	0.0000	0.0000	0.0000	0.0000	0.0053	4.2958	0.0000	0.0000
2,2	0.0000	3.2503	0.0000	0.0000	0.0000	0.0000	0.0000	0.0000	0.0000	0.0000	9.9655	0.0000
2,1	0.0000	0.0000	0.0000	-0.0001	0.0000	3.8686	0.0002	0.0000	0.0000	0.0000	0.0000	8.2956

cylindrical tank contains fresh water with a density of 1000 kg/m^3 . The circular plate under investigation is clamped at its edge and analytically investigated by Amabili and Dalpiaz [19], Amabili [20], and Chiba [21].

Table 5
Vibration modes of a clamped circular plate

ij	0	1	2
0			
1			
2			

The mode shapes of the circular plate may be identified with two integers. These integers, i and j , are considered as the number of nodal diameters and nodal circles, respectively (see Table 5). A nodal line gives the same condition as a fixed boundary. For example, the first mode shape ($i = 0, j = 0$) in Table 5 has no nodal diameter or nodal circle. Therefore, the whole plate vibrates about its equilibrium plane in this particular mode shape.

The in vacuo dynamic properties, e.g., natural frequencies and mode shapes, were obtained by use of ANSYS finite element software. The clamped circular plate was discretized by four-noded, quadrilateral shell elements. In order to test the convergence of the in vacuo results, three different finite element idealizations were considered. These idealizations consist of 129, 289 and 513 finite elements distributed over the circular plate structure. Table 6 shows the convergence of the finite element predictions, and the analytically calculated in vacuo frequencies [22]. As seen in Table 6, the natural frequency values are slowly converging with increasing number of elements. The predictions based on the 513 finite element idealization compare well with the analytical calculations (1.5% maximum difference), for nine in vacuo modes presented in Table 6. Therefore, this final idealization was used for the in vacuo dynamic characteristics of the plate structure.

Another study was performed to test the convergence of the hydrodynamic properties. It should be noted that the structural and fluid idealizations are independent of one another, both depending on the complexity of the structure and the convergence of the results. The hydrodynamic panels were distributed over the wetted surface of the plate structure as follows: one structural element corresponding to one hydrodynamic panel. In addition hydrodynamic

Table 6
Convergence of FEM natural frequencies (in vacuo) for clamped circular plate (Hz)

Mode (<i>i,j</i>)	129 elements idealization	289 elements idealization	513 elements idealization	Analytical
0,0	234.7	238.1	238.7	239.5
1,0	494.0	496.4	497.2	498.4
2,0	802.5	810.2	813.2	817.8
0,1	911.4	921.5	925.8	932.4
1,1	1395.1	1411.3	1417.6	1425.9
2,1	1920.1	1950.7	1963.6	1983.0
0,2	2017.7	2050.0	2064.7	2089.0
1,2	2711.6	2764.9	2785.6	2815.3
2,2	3433.1	3516.8	3552.0	3606.1

Table 7
Convergence of *wet* natural frequencies of clamped circular plate in a rigid cylindrical tank (Hz)

Mode (<i>i,j</i>)	<i>d/r</i> = 0.5			<i>d/r</i> = 1		
	209 panels idealization	409 panels idealization	673 panels idealization	289 panels idealization	529 panels idealization	833 panels idealization
0,0	111.6	112.7	112.8	90.6	91.3	91.3
1,0	269.4	265.9	264.6	252.5	248.8	247.4
2,0	501.6	486.7	481.4	493.3	478.0	472.6
0,1	543.1	541.1	540.6	517.6	515.5	515.1
1,1	923.3	908.1	902.5	907.5	892.0	886.3
2,1	1394.1	1356.1	1341.6	1387.5	1348.9	1334.3
0,2	1417.9	1399.9	1393.9	1393.1	1376.5	1372.3
1,2	2045.9	2007.8	1991.3	2031.4	1993.3	1976.9
2,2	2762.7	2689.7	2659.4	2757.0	2683.6	2652.9

panels were also distributed over the wetted surface of the rigid cylindrical tank, in order to impose the boundary condition $\partial\Phi/\partial\mathbf{n} = 0$ at the fluid–rigid wall interface. For the results presented in Table 7, 209, 409 and 673 hydrodynamic panels were adopted separately over the wetted surfaces (plate and rigid cylindrical wall) for the filling ratio $d/r = 0.5$, and 289, 529 and 833 hydrodynamic panels for the filling ratio $d/r = 1$. In the first group of idealizations (209 and 289 panel idealizations), 129 hydrodynamic panels were distributed over the wetted plate, and 80 and 160 hydrodynamic panels were adopted over the wetted cylindrical surface, respectively, for the filling ratios $d/r = 0.5$ and 1. In the second group of idealizations (409 and 529 panel idealizations), the number of panels over the wetted plate was increased to 289. For this group of idealizations, 120 and 240 hydrodynamic panels were adopted over the wetted cylindrical surface, respectively, for the filling ratios $d/r = 0.5$ and 1. Finally, the third group of idealizations (673 and 833 panel idealizations) involves 513 hydrodynamic panels distribution over the wetted plate, and 160 and 320 hydrodynamic panels distribution over the wetted cylindrical surface for the filling ratios $d/r = 0.5$ and 1, respectively. From the results presented in Table 7, it can be seen that the *wet* frequencies show a dependence on the number of hydrodynamic panels distributed. However,

Table 8

Comparisons of *wet* natural frequencies of clamped circular plate in a rigid cylindrical tank (Hz)

Mode (<i>i, j</i>)	<i>d/r</i> = 0.1			<i>d/r</i> = 0.5			<i>d/r</i> = 1			<i>d/r</i> = 2	
	This study	Chiba [21]	Amabili and Dalpiaz [19]	This study	Chiba [21]	Amabili and Dalpiaz [19]	This study	Chiba [21]	Amabili and Dalpiaz [19]	This study	Amabili [20]
0,0	173.5	177	176.8	112.8	110	114.5	91.3	92	91.7	71.8	69.1
1,0	365.7	—	—	264.6	—	—	247.4	—	—	244.2	241.0
0,1	688.1	694	700.7	540.6	540	547.3	515.1	520	519.8	499.5	495.7
1,1	1072.3	—	—	902.5	—	—	886.3	—	—	883.6	871.9
0,2	1585.2	1620	1609.7	1393.9	1410	1408.7	1372.3	1390	1385.0	1356.2	1349.7
1,2	2183.0	—	—	1991.3	—	—	1976.9	—	—	1974.5	1943.7

the differences between the results based on the last two groups of idealizations are practically negligible. For the results presented in Table 8, 545, 673, 833 and 1153 hydrodynamic panels were adopted over the wetted plate and cylindrical surfaces, respectively, for the filling ratios $d/r = 0.1, 0.5, 1$ and 2 . An additional convergence study was also performed in order to establish the number of in vacuo modes needed for the predictions. As a result of this study, a number of 32 in vacuo principal modes were included in the calculations.

The flexible plate structure adopted in this study was considered as a bottom plate for a rigid circular cylindrical tank, and its natural frequencies and associated mode shapes were calculated for various filling ratios (d/r). Table 8 compares the results of this study with those of Chiba [21], Amabili and Dalpiaz [19] and Amabili [20]. There is a very good overall agreement between the results presented. However, there are some differences between the results of the present study and those found in the literature. These differences lie in the range between 0.1% and 2.5% in comparison with the predictions of Chiba [21], and 0.4% and 3.9% when compared with the predictions of Amabili and Dalpiaz [19] and Amabili [20]. It should be noted that, for the filling ratio $d/r = 2$, the natural frequencies presented for Amabili [20] in Table 8 were calculated by use of the NAVMI matrices given in Amabili [20]. As seen from Table 8, the *wet* natural frequencies decrease with increasing filling ratio d/r . Therefore, the minimum frequencies were calculated for the filling ratio $d/r = 2$.

The calculations were repeated for various filling ratios d/r , and they are presented for the nodal diameters $i = 0, 1, 2, 3$ and nodal circles $j = 0, 1, 2$ in Fig. 6. It can be observed from Fig. 6 that the *wet* natural frequencies decrease in value until they reach a constant value at higher filling ratios (d/r). Meanwhile, the *wet* frequencies increase with increasing number of nodal diameters and nodal circles for a given filling ratio. Therefore, the highest frequencies were obtained for the mode shape with $i = 3$ and $j = 2$.

3.3. A flexible cylindrical shell with flexible end plates (hermetic can)

The final case study involves the vibration of a flexible circular cylindrical shell and two flexible circular plates connected to the shell at its ends. The shell–plate system (hermetic can) is assumed

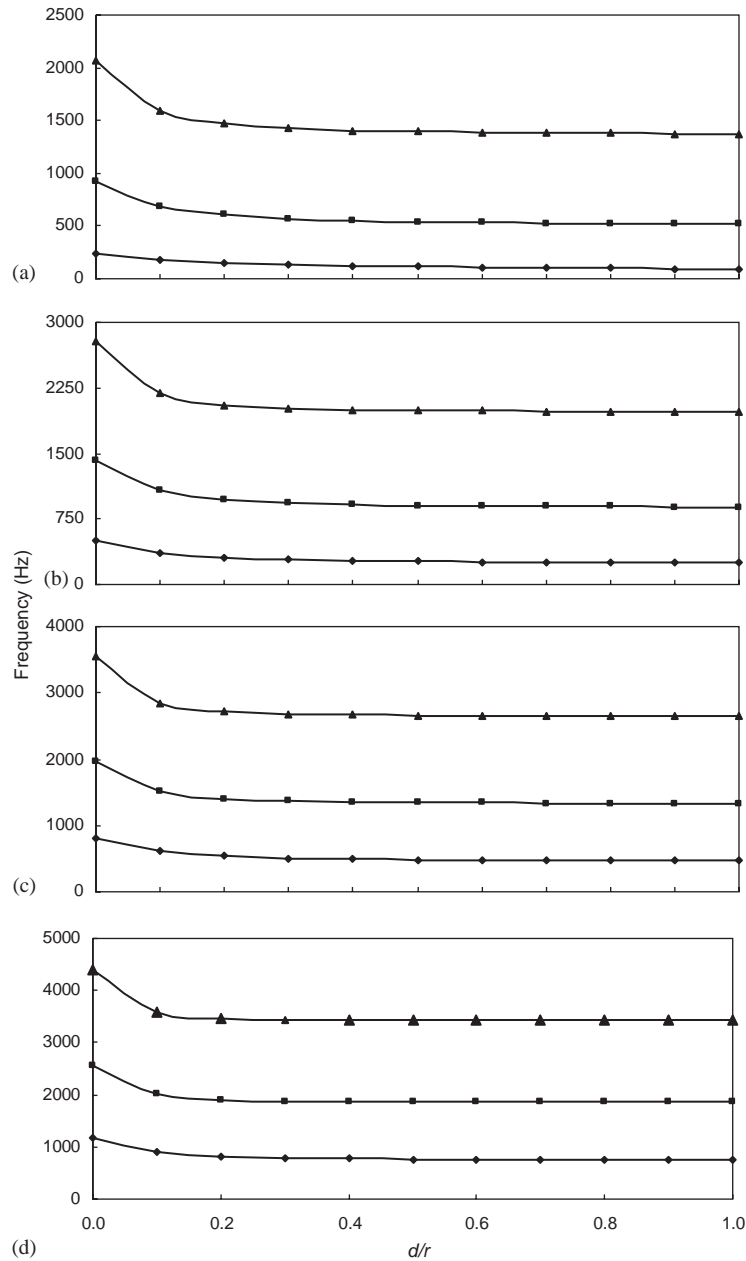


Fig. 6. Wet frequencies of clamped circular plate in a rigid cylindrical tank as a function of filling ratio (d/r): (a) $i = 0$; (b) $i = 1$; (c) $i = 2$; (d) $i = 3$. Key: $-\blacklozenge-$, $j = 0$; $-\blacksquare-$, $j = 1$; $-\blacktriangle-$, $j = 2$.

as simply supported at the base, and have the following dimensions and material properties: mean radius, $r = 0.1$ m, length, $L = 0.2$ m, thickness, $t = 0.002$ m, Young's modulus, $E = 206$ GPa, density, $\rho = 7850$ kg/m³, and Poisson ratio, $\nu = 0.3$. The hermetic can under investigation is

completely filled with fresh water having $\rho_f = 1000 \text{ kg/m}^3$, and it was analytically studied by Amabili [23] and Huang and Soedel [24].

A particular mode shape of the shell–plate system is identified with the displacement wave forms of the cylindrical shell and circular end plates. However, the mode shapes are generally dominated either by the displacements of the cylindrical shell or by those of the end plates. Therefore, the mode shapes of the shell–plate system are separated into two groups: the shell-dominant and plate-dominant modes. The shell-dominant modes may be identified with the number of standing waves around the circumference, n , and the number of standing half-waves, m , along the cylindrical shell. A combination of n and m forms a particular shell-dominant mode shape (n, m) . The plate-dominant principal mode shapes, on the other hand, identified with two integers, i and j , which are considered as the number of nodal diameters and nodal circles, respectively (see Table 5). A nodal line gives the same condition as a fixed boundary.

The mode shapes of the shell–plate system are, further, divided into two distinct groups: the symmetric and anti-symmetric mode shapes. The empty or completely-filled can is symmetric with respect to the plane $x = L/2$ (see Fig. 2). Therefore, the mode shapes are either symmetric or anti-symmetric with respect to this plane. A symmetric mode shape shows similar displacement characteristics on either side of the plane $x = L/2$. On the other hand, an anti-symmetric mode shape exhibits opposite displacement behaviour about the same plane.

The in vacuo dynamic properties of the empty shell–plate system were calculated by use of ANSYS. Three different idealizations were considered in order to obtain the converged in vacuo and *wet* dynamic properties (i.e., frequencies and mode shapes) of the structure. The predicted *dry* and *wet* natural frequencies are shown in Table 9 for the circumferential wave number (or nodal diameter number) 4. In the first in vacuo idealization, 48 and 20 equally spaced elements were distributed, respectively, around the circumference and along the cylindrical shell. On the other hand, each circular end plate was discretized by use of 289 quadratic shell elements. Therefore, a total number of 1538 finite elements was used in the first idealization. The second in vacuo idealization involves 2946 elements distribution-64 elements around the circumference, 30 elements along the length, and 513 elements over each end. Finally, for a third in vacuo idealization, the number of elements around the circumference was increased to 80, and the

Table 9
Convergence of *dry* and *wet* natural frequencies (Hz) of hermetic can for n (or i) = 4

No	Dry analysis			Wet analysis		
	1538 elements idealization	2946 elements idealization	4002 elements idealization	1538 panels idealization	2946 panels idealization	4002 panels idealization
1	1358.9	1358.6	1358.4	899.1	888.4	883.6
2	3085.7	3099.9	3105.5	2259.0	2225.3	2211.9
3	3120.1	3140.9	3149.5	2351.3	2334.2	2323.4
4	3340.6	3341.4	3340.7	2355.0	2336.3	2325.6
5	5076.3	5071.7	5059.9	3645.9	3581.4	3556.6
6	6139.2	6172.7	6177.5	4838.9	4753.7	4719.9
7	6266.3	6314.7	6335.2	5299.7	5218.0	5169.4
8	6571.5	6607.3	6605.4	5309.3	5228.1	5180.1

number of elements along the shell was kept as in the second idealization. The number of elements over each end was increased to 801. As a result of this final idealization, 4002 finite elements were distributed over the cylindrical shell and end plates. The in vacuo natural frequencies in Table 9 converge with increasing number of finite elements, and there are negligible differences between the results of the last two idealizations. Therefore, the in vacuo dynamic properties, e.g., natural frequencies and associated mode shapes, of the last idealization were adopted in this study. On the other hand, a maximum number of 96 in vacuo principal modes were included in the calculations.

Another convergence analysis was performed for the *wet* dynamic properties of the shell–plate system. The cylindrical tank was assumed completely filled with water. The hydrodynamic panels were distributed over the wetted surface of the shell–plate system as follows: one structural element (finite element) corresponding to one hydrodynamic panel. Therefore, the same number of hydrodynamic panels and structural elements were adopted for the *wet* results presented in this study (see Table 9). It can be observed from Table 9 that the *wet* frequencies are converging slowly with increasing number of hydrodynamic panels. The final panel idealization was adopted for the calculations, and it involves 80 hydrodynamic panels distributed around the circumference, 30 hydrodynamic panels distributed along the cylindrical shell and 801 hydrodynamic panels distributed over each end.

The calculated in vacuo and *wet* frequencies are presented in Tables 10 and 11, respectively, for the plate-dominant and shell-dominant modes. The predictions of this study are compared with the analytical calculations of Huang and Soedel [24] in the *dry* analysis, and with those of Amabili [23] in the *wet* analysis, as seen in Tables 10 and 11. It should also be noticed that the mode shapes in Tables 10 and 11 are classified as symmetric (S) and anti-symmetric (A), with respect to the plane $x = L/2$.

For the plate-dominant modes, the predicted in vacuo frequencies compare well with those of Huang and Soedel [24] in Table 10. However, there are some differences between the results. These differences lie in the range between 0.3% and 4.7%, except for the mode shape ($i = 0, j = 0$). For the symmetric and anti-symmetric mode shapes ($i = 0, j = 0$), the finite element predictions are, respectively, 11.2% and 23.7% higher than those analytically calculated by Huang and Soedel [24], in which similar discrepancies were observed between their predictions based on the receptance method and finite element calculations. On the other hand, the predicted *wet* frequencies in Table 10 show a maximum difference of 5.1% in comparison with the analytical calculations of Amabili [23], except for the anti-symmetric mode shape ($i = 0, j = 0$). It should also be noted that there is no results presented for the plate-dominant symmetric modes ($i = 0, j = 0$) and ($i = 0, j = 1$) in Table 10. This is because of that the above mentioned mode shapes do not satisfy the incompressibility condition (18) for the completely-filled structure. Therefore, they were excluded from the calculations in this study.

Table 11 presents the predicted *dry* and *wet* natural frequencies of the hermetic can for the shell-dominant modes. As seen in Table 11, the in vacuo natural frequency predictions compare very well with those of Huang and Soedel [24]. The differences are in the range between no difference and 1.9%. The predicted *wet* natural frequencies are also in good comparison with the results of Amabili [23], except for the symmetric mode shape ($n = 1, m = 1$). For this particular mode shape, the predicted *wet* frequency value is 32.9% higher than that calculated by Amabili [23]. Unfortunately, there is no explanation found for the occurrence of this particular discrepancy. It should also be said that the symmetric mode shapes ($n = 0, m = 1$) and ($n = 0, m = 3$) do not

Table 10
 Comparisons of *dry* and *wet* natural frequencies for plate-dominant modes (hermetic can) (Hz)

Mode (<i>i,j</i>)	Dry analysis						Wet analysis					
	Symmetric			Antisymmetric			Symmetric			Antisymmetric		
	This study	Huang and Soedel [24]	(%)	This study	Huang and Soedel [24]	(%)	This study	Amabili [23]	(%)	This study	Amabili [23]	(%)
0,0	454.6	408.9	11.2	505.7	408.7	23.7	—	—	—	259.0	210	23.3
0,1	1783.4	1771.9	0.6	1855.1	1771.4	4.7	—	1070	—	1194.3	1170	2.1
1,0	955.0	940.9	1.5	952.8	940.8	1.3	518.9	545	4.8	531.6	560	5.1
1,1	2754.8	2771.5	0.6	2726.2	2771.4	1.6	1906.9	—	—	1918.0	1980	3.2
2,0	1569.3	1576.0	0.4	1568.4	1577.9	0.6	998.0	1050	5.0	1003.9	1050	4.4
2,1	3820.0	3886.4	1.7	3813.1	3876.1	1.6	2893.4	2950	1.9	2853.3	2925	2.5
3,0	2306.7	2342.9	1.5	2303.3	2326.1	1.0	1608.5	1638	1.8	1603.1	1637	2.1
3,1	5030.5	5125.1	1.8	5007.9	5080.4	1.4	3947.7	3977	0.8	3968.4	3976	0.2
4,0	3149.5	3194.9	2.4	3105.5	3096.5	0.3	2323.4	2390	2.8	2325.6	2400	3.1
4,1	6335.2	6454.5	1.8	6177.5	6222.6	0.7	5169.4	5200	0.6	5180.1	5250	1.3
5,0	4061.9	4086.6	0.6	4115.4	4187.2	1.7	3154.7	3320	5.0	3161.6	3230	2.1
5,1	7732.2	7869.9	1.7	7915.5	8244.0	4.0	6529.7	6600	1.1	6480.7	6430	0.8

Table 11
Comparisons of *dry* and *wet* natural frequencies for shell-dominant modes (hermetic can) (Hz)

Mode (n, m)	Mode type	Dry analysis			Wet analysis		
		This study	Huang and Soedel [24]	(%)	This study	Amabili [23]	(%)
0,1	S	7962.6	7912.0	0.6	—	2360	—
0,2	A	8125.7	8151.0	0.3	4018.7	4025	0.2
0,3	S	8206.0	8274.0	0.8	—	4875	—
0,4	A	8378.0	8508.0	1.5	5638.1	5645	0.1
1,1	S	4897.9	4898.6	0.0	2498.5	1880	32.9
1,2	A	7247.3	7264.5	0.2	3825.8	3745	2.2
1,3	S	7818.2	7878.0	0.8	4931.6	4790	3.0
1,4	A	8129.3	8235.0	1.3	5668.2	5540	2.3
2,1	S	2810.5	2816.7	0.2	1568.6	1445	8.6
2,2	A	5629.6	5637.9	0.1	3356.8	3225	4.1
2,3	S	6781.1	6856.7	1.1	4507.1	4400	2.4
2,4	A	7721.6	7865.0	1.8	5369.7	5295	1.4
3,1	S	1734.7	1734.8	0.0	1050.2	1011	3.9
3,2	A	4225.0	4224.5	0.0	2687.2	2601	3.3
3,3	S	5962.4	5997.0	0.6	4029.6	3914	3.0
3,4	A	7041.8	7101.7	0.8	5056.4	4957	2.0
4,1	S	1358.4	1369.1	0.8	883.6	865	2.2
4,2	A	3340.7	3406.1	1.9	2211.9	2155	2.6
4,3	S	5059.9	5072.4	0.2	3556.6	3485	2.1
4,4	A	6605.4	6727.8	1.8	4719.9	4625	2.1
5,1	S	1482.2	1493.7	0.8	1019.8	1000	2.0
5,2	A	2831.5	2840.9	0.3	2000.8	1960	2.1
5,3	S	4533.6	4597.7	1.4	3266.2	3115	4.9
5,4	A	5950.7	5986.0	0.6	4485.5	4410	1.7

satisfy the incompressibility condition (18), and, therefore, there is no results presented for these particular mode shapes in Table 11.

Fig. 7 presents the predicted *wet* modes of the completely-filled tank for the circumferential wave number (or nodal diameter number) 3. The mode shapes shown in Fig. 7 are evaluated by using Eq. (27). As seen in Fig. 7, the predicted mode shapes and associated *wet* frequencies compare well with those obtained by Amabili [23]. The plate- and shell-dominant modes can be clearly identified, and all the mode shapes satisfy the incompressibility condition (18). On the other hand, it should be noticed that the mode shapes are either symmetric or anti-symmetric with respect to the plane $x = L/2$.

4. Conclusions

The dynamic characteristics (*wet* natural frequencies and associated modes) of fluid storage tanks, partially or completely filled with fluid, were calculated by an approach based on the boundary-integral equation method and the method of images. It can be concluded from the

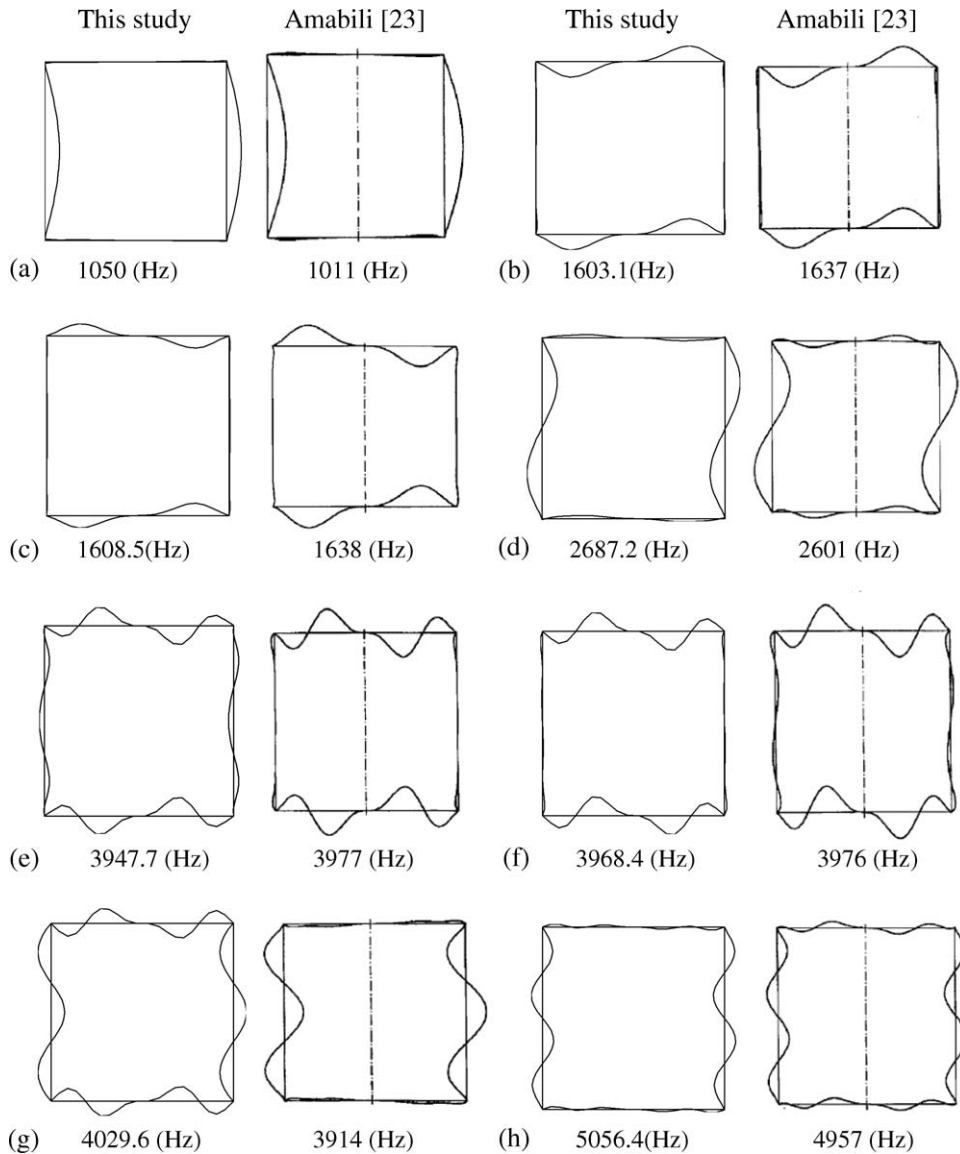


Fig. 7. Comparisons of predicted wet mode shapes of completely filled hermetic can for n (or i) = 3: (a) first symmetric shell-dominant mode; (b) first anti-symmetric plate-dominant mode; (c) first symmetric plate-dominant mode; (d) first anti-symmetric shell-dominant mode; (e) second symmetric plate-dominant mode; (f) second anti-symmetric plate-dominant mode; (g) second symmetric shell-dominant mode; (h) second anti-symmetric shell-dominant mode.

results presented that the method proposed is suitable for the vibration analysis of fluid containing elastic structures.

Three different test cases were considered in this study. These are (i) a clamped–free cylindrical tank with a rigid bottom, (ii) a flexible bottom plate in a rigid cylindrical tank, and (iii) a flexible cylindrical shell with flexible end plates (hermetic can). For the first two test cases, the influence of

the contained fluid on the dynamic response behaviour of the structures was demonstrated for various filling depths. However, the hermetic can considered in the final test case was assumed completely filled with water. From the results presented, it can be seen that the calculations based on the present method generally show very good agreement with the available experimental and numerical data. However, some large discrepancies were observed in comparison with the available numerical data, especially for the hermetic can.

Throughout the calculations, the normal velocities on the wetted surfaces were expressed in terms of modal structural displacements, obtained from the in vacuo dynamic analysis. However, it should be noted that the normal fluid velocities cannot be arbitrarily specified. They have to satisfy the incompressibility condition (18). The mode shapes not satisfying this condition were excluded from the calculations. This happened for some symmetric modes of the completely filled hermetic can (see Section 3.3). It must be realized that the method employed in this study cannot take into account the effect of compressibility.

The structural and fluid idealizations are independent and both depending on the complexity of the structure and the convergence of the results. To test the convergence of the wet dynamic characteristics various numbers of hydrodynamic panels and in vacuo principal modes were adopted in the calculations. It is realized from the results presented (see, for example, Table 9) that the wet frequency predictions converge slowly with increasing number of hydrodynamic panels. On the other hand, a considerable number of in vacuo principal modes should be included in the calculations when the number of wet modes of interest is large. For instance, for the results presented for the hermetic can in Tables 10 and 11, a number of 96 in vacuo principal modes was adopted in the calculations.

As seen from the generalized added masses presented in Table 4, there is coupling between the in vacuo modes. This is because of that, the hydrodynamic pressure distribution does not have necessarily the same spatial distribution as those of the in vacuo principal modes. Therefore, this produces hydrodynamic coupling between the in vacuo modes.

It can be seen from the results presented that the frequency values behave as expected. That is to say that the frequencies decrease with increasing area of contact with fluid. Therefore, the lowest frequencies occurred for the cases in which the structures have the largest area of contact with fluid.

The present work has demonstrated the versatility of the method developed through three different test studies. In a future study, the effect of a flowing fluid on the dynamic characteristics of elastic structures will be considered.

Acknowledgements

This research was financially supported by the Scientific and Technical Research Council of Turkey (TUBITAK Project No: 102I028). This support is gratefully acknowledged.

References

- [1] S.P. Lim, M. Petyt, Free vibration of a cylinder partially filled with a liquid, *Proceedings of the International Conference on Recent Advances in Structural Dynamics*, Institute of Sound and Vibration, Southampton University, 7–11 July 1980, pp. 447–455.

- [2] L.G. Olson, K.J. Bathe, Analysis of fluid–structure interactions, A direct symmetric coupled formulation based on the fluid velocity potential, *Computers and Structures* 21 (1985) 21–32.
- [3] R. Ohayon, R. Valid, True symmetric variational formulations for fluid–structure interaction in bounded domains-finite element results, in: R.W. Lewis, P. Bettess, E. Hinton (Eds.), *Numerical Methods in Coupled Systems*, Wiley, New York, 1984, pp. 293–325.
- [4] H.J.-P. Morand, R. Ohayon, *Fluid Structure Interaction*, John Wiley and Sons, Paris, 1995.
- [5] T. Mazúch, J. Horáček, J. Trnka, J. Veselý, Natural modes and frequencies of a thin clamped–free steel cylindrical storage tank partially filled with water: FEM and measurements, *Journal of Sound and Vibration* 193 (1996) 669–690.
- [6] Y.L. Zhang, D.G. Gorman, J.M. Reese, A finite element method for modelling the vibration of initially tensioned thin-walled orthotropic cylindrical tubes conveying fluid, *Journal of Sound and Vibration* 245 (2001) 93–112.
- [7] U. Röhr, P. Möller, Hydroelastic vibration analysis of wetted thin-walled structures by coupled FE-BE-procedure, *Structural Engineering and Mechanics* 12 (2001) 101–118.
- [8] G.V. Mysore, S.I. Liapis, R.H. Plaut, Dynamic analysis of single-anchor inflatable dams, *Journal of Sound and Vibration* 215 (1998) 251–272.
- [9] A. Ergin, W.G. Price, R. Randall, P. Temarel, Dynamic characteristics of a submerged, flexible cylinder vibrating in finite water depths, *Journal of Ship Research* 36 (1992) 154–167.
- [10] A. Nestegård, M. Mejlænder-Larsen, Hydrodynamic added mass of a floating vibrating structure, in: O. Faltinsen, et al. (Eds.), *Hydroelasticity in Marine Technology*, A.A. Balkema, Rotterdam, 1994, pp. 261–272.
- [11] A. Ergin, P. Temarel, Free vibration of a partially liquid-filled and submerged, horizontal cylindrical shell, *Journal of Sound and Vibration* 254 (2002) 951–965.
- [12] ANSYS, User’s manual, ANSYS, Inc., Houston, TX, 1994.
- [13] K.-J. Bathe, E.L. Wilson, *Numerical Methods in Finite Element Analysis*, Prentice-Hall, Englewood Cliffs, NJ, 1976.
- [14] A. Ergin, The response behaviour of a submerged cylindrical shell using the doubly asymptotic approximation method (DAA), *Computers and Structures* 62 (1997) 1025–1034.
- [15] M. Amabili, M.P. Paidoussis, A.A. Lakis, Vibrations of partially filled cylindrical tanks with ring-stiffeners and flexible bottom, *Journal of Sound and Vibration* 213 (1998) 259–299.
- [16] F. Kito, *Principles of Hydro-Elasticity*, Keio University Publications, Tokyo, 1970.
- [17] J.L. Hess, A.M.O. Smith, Calculation of potential flow about arbitrary bodies, in: D. Küchemann, et al., (Eds.), *Progress in Aeronautical Sciences*, Vol. 8, Pergamon Press, New York, 1967, pp. 1–138.
- [18] J.L. Hess, Review of integral-equation techniques for solving potential-flow problems with emphasis on the surface-source method, *Computer Methods in Applied Mechanics and Engineering* 5 (1975) 145–196.
- [19] M. Amabili, G. Dalpiaz, Vibrations of base plates in annular cylindrical tanks: theory and experiments, *Journal of Sound and Vibration* 210 (1998) 329–350.
- [20] M. Amabili, Bulging modes of circular bottom plates in rigid cylindrical containers filled with a liquid, *Shock and Vibration* 4 (1997) 51–68.
- [21] M. Chiba, Nonlinear hydroelastic vibration of a cylindrical tank with an elastic bottom, containing liquid, Part II: linear axisymmetric vibration analysis, *Journal of Fluids and Structures* 7 (1993) 57–73.
- [22] A.W. Leissa, *Vibration of Plates*, NASA SP-160, U.S Government Printing Office, Washington, DC, 1969.
- [23] M. Amabili, Vibrations of fluid-filled hermetic cans, *Journal of Fluids and Structures* 14 (2000) 235–255.
- [24] D.T. Huang, W. Soedel, On the free vibrations of multiple plates welded to a cylindrical shell with special attention to mode pairs, *Journal of Sound and Vibration* 166 (1993) 315–339.